

PAPER • OPEN ACCESS

Detailed band alignment of high-B-composition BGaN with GaN and AlN

To cite this article: F AlQatari *et al* 2023 *J. Phys. D: Appl. Phys.* **56** 385305

View the [article online](#) for updates and enhancements.

You may also like

- [Marker Pen Lithography for Flexible and Curvilinear on-Chip Energy Storage](#)
Narendra Kurra, Qiu Jiang and Husam Alshareef
- [Pt Surfaces Modified with Mo Species as an Improved Electrocatalyst for Efficient Water Splitting](#)
Angel Tonatiah Garcia-Esparza, Tatsuya Shinagawa and Kazuhiro Takanabe
- [Improving the Performance of SOFC Anodes by Decorating Perovskite with Ni Nanoparticles](#)
Samir Bouffrad, Mark Cassidy, Enrico Traversa et al.

Detailed band alignment of high-B-composition BGaN with GaN and AlN

F AlQatari^{1,*} , C-H Liao¹, R R Aguilera-Vazquez¹, X Tang¹ , S Lopatin^{2,*} and X Li^{1,*} 

¹ Advanced Semiconductor Laboratory, Electrical and Computer Engineering Program, CEMSE Division, King Abdullah University of Science and Technology (KAUST), Thuwal 23955-6900, Saudi Arabia

² Imaging and Characterization Core Laboratory, King Abdullah University of Science and Technology (KAUST), Thuwal 23955-6900, Saudi Arabia

E-mail: feras.alqatari@kaust.edu.sa, sergei.lopatin@gmail.com and xiaohang.li@kaust.edu.sa

Received 5 April 2023, revised 30 May 2023

Accepted for publication 6 June 2023

Published 23 June 2023



Abstract

The electronic structure of $B_{0.097}Ga_{0.903}N$ was determined by examining its bandgap and valence band offset (VBO) in detail. The BGaN sample was grown using a horizontal reactor metalorganic chemical vapor deposition. For bandgap determination, three different techniques were utilized yielding similar results, which are: UV–Vis spectroscopy, Schottky photodiodes, and electron energy-loss spectroscopy. The bandgap was determined to be ~ 3.55 eV. For measuring the VBO, the valence edges and the core levels of Al 2s and Ga 2p were measured using x-ray photoelectron spectroscopy (XPS). The valence edges were then fitted and processed along with the core levels using the standard Kraut method for VBO determination with AlN. The BGaN/AlN alignment was found to be -1.1 ± 0.1 eV. Due to core level interference between GaN and BGaN, the Kraut method fails to provide precise VBO for this heterojunction. Therefore, a different technique is devised to analyze the measured XPS data which utilizes the alignment of the Fermi levels of the BGaN and GaN layers when in contact. Statistical analysis was used to determine the BGaN/GaN alignment with decent precision. The value was found to be -0.3 ± 0.1 eV.

Supplementary material for this article is available [online](#)

Keywords: band alignment, BGaN, XPS

(Some figures may appear in colour only in the online journal)

1. Introduction

A semiconductor's bandgap may be its single most important property, especially when designing the simplest devices made of single-material homojunctions. However, as soon as

heterojunctions are introduced, the bandgap alone becomes insufficient in describing the behavior of carriers and photons in the desired structure. The reason being that the electronic structure of the junction can have one of three band alignment types: type-I (straddling gap), type-II (staggered gap), and type-III (broken gap). This can occur even when other factors such as surface states and polarization charges are not explicitly considered [1, 2]. Therefore, the band alignment at a heterojunction becomes the second most important property needed to understand the behavior of the junction [3]. Typically, at least three quantities are needed to model a junction's band structure: the two bandgaps of the constituent

* Authors to whom any correspondence should be addressed.



Original content from this work may be used under the terms of the [Creative Commons Attribution 4.0 licence](#). Any further distribution of this work must maintain attribution to the author(s) and the title of the work, journal citation and DOI.

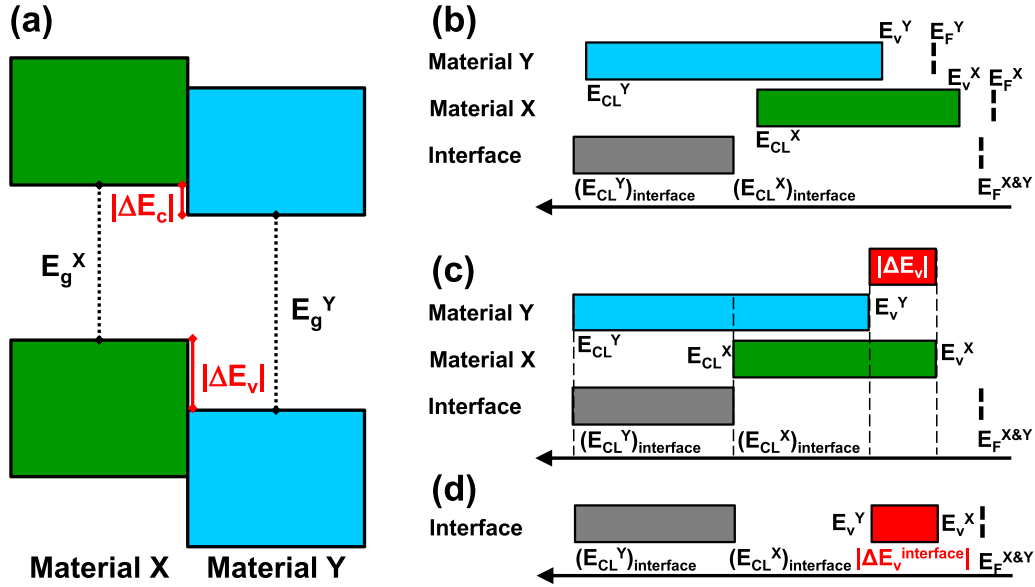


Figure 1. (a) Flat band model of type-II alignment of materials X and Y showing the relationship between the quantities in equation (1). (b) Schematic showing energy levels typically measured when aligning bands using equation (2). Notice the different Fermi levels (E_F) for each sample. (c) The resulting VBO (in red) when the energy levels are aligned. The Fermi level of the interface sample is highlighted as an effective reference energy. (d) The valence energies of the interface sample can be measured for alignment using equation (3). The arrows in (b)–(d) point in the direction of increasing binding energy.

materials, and the way they are aligned, described by the valence band offset (VBO). Figure 1(a) shows a simple schematic for a band structure with a type-II alignment. Equation (1) describes how the gaps are related to the alignment. The equation takes the gaps and the VBO to give the conduction band offset (CBO) relating all the quantities figure 1(a):

$$\Delta E_c = \Delta E_v + E_g^Y - E_g^X \quad (1)$$

where Δ is the offset of the conduction bands minima (E_c) and the valence bands maxima (VBM, E_v), and E_g is the bandgap of material X or material Y on either side of the junction.

X-ray photoelectron spectroscopy (XPS) is the most used technique to determine the VBO of different heterojunctions [4, 5]. Using XPS, direct measurements of core-level and valence-edge energies can be performed. To determine the VBO from these measurements, equation (2) is typically used which is commonly referred to as the Kraut method [6]:

$$\Delta E_v = (E_{CL}^Y - E_v^Y) - (E_{CL}^X - E_v^X) - (E_{CL}^Y - E_{CL}^X)_{interface} \quad (2)$$

where E_{CL} are chosen core levels of each material X and Y. The first four terms are measured for thick samples of X and Y typically referred to as ‘bulk’ samples. The last two terms are measured for a heterojunction between them referred to as an ‘interface’ sample. The use of this equation allows for the determination of the VBO of the two bulk samples taking into consideration band bending due to interface states and other sources.

Unfortunately, the Kraut method can only work when the measurement can discern between the core levels of the two materials. An example of an interface where the Kraut method is not easily applicable is that between a semiconductor and

its oxide. One solution for that issue is to simply measure the valence edges of the semiconductor and its oxide and take the difference between them as in equation (3):

$$\Delta E_v^{interface} = (E_v^X - E_v^Y)_{interface} \quad (3)$$

This approach has been utilized by the others to study the Si/SiO₂ interface [7, 8]. An advantage of this method is its simplicity since only the low binding energy region of a single interface sample is needed to be measured. The physics behind this method is that the Fermi levels of materials X and Y become one when they are in physical contact. However, this method lacks the advantages of the Kraut method which gives the VBO of the bulk instead of at the interface. Therefore, strain and interface states may influence the results using this method. Figures 1(b)–(d) summarize the two methods schematically.

In the past half century, III-nitrides have gained high popularity mainly due to their now commercial applications in optoelectronics and, more recently, power electronics. An emerging class of III-nitrides are those alloyed with boron (B). B alloying can be used to tune several properties including the bandgap and band alignment. A recent work by Mickevičius *et al* has shown that low B composition BGaN and GaN have a type-II alignment [9]. However, the value provided in this study is not quantitative due to the used approximations and lack of reference energy.

Recently, the growth of B_xGa_{1-x}N at a high B composition ($x > 10\%$) has been reported [10]. Therefore, in this work, we study the electronic properties of BGaN at a similar composition ($x \sim 9.7\%$). The bandgap and the band alignments of B_{0.097}Ga_{0.903}N with AlN and GaN are examined in detail. The BGaN/AlN is studied due to its straightforwardness and as a

cross-validation to the BGaN/GaN interface. The latter interface is intriguing from both a physics perspective due to the lack of distinguishable core levels and VBM, and an application perspective, as GaN is more advanced in devices such as power electronics and optoelectronics [11–14].

In the process, we enhance the precision of the method in equation (3) to be the same as the precision of the XPS instrument. Finally, combining the bandgap and band alignment data is used to create a complete band structure of the two heterojunctions using the flat band model.

2. Experimental methods

The high B composition BGaN and the AlN and GaN used in the alignment were grown using a horizontal reactor metalorganic chemical vapor deposition from Taiyo Nippon Sanso on metal-polar (0002)-oriented thick ($>1.5\ \mu\text{m}$) AlN/sapphire (or GaN/sapphire) templates. The metalorganic compounds used were trimethylaluminum, triethylborane and trimethylgallium as the sources for Al, B, and Ga, respectively. Ammonia was the source for N in the reactor. Hydrogen gas was used as a carrier for the reactants. For the BGaN layer, high V/III and B/III ratios of 4100 and 0.51 were used, respectively. Low growth temperature and pressure of 650 °C and 75 Torr were used, respectively.

The B composition of the BGaN layer is estimated by linear interpolation of lattice parameters as estimated by the Bruker D2 Phaser x-ray diffraction (XRD) [15]. The bandgaps of the different layers were estimated using three different techniques:

- UV–Vis transmittance spectrum of a 120 nm film measured using a Thermo Scientific Evolution 160. Tauc plot for the estimation of the optical bandgap was utilized [16].
- Additionally, a simple metal-semiconductor-metal (MSM) interdigitated photodetector was created to confirm the optical bandgap [17]. The detector's responsivity was measured using a Zolix photodetector measurement system. The detector covers an area of $500 \times 500\ \mu\text{m}^2$ with each finger having a width and an interdigital distance of 30 μm . The contact is Au/Ti with thicknesses of 200/20 nm.
- Furthermore, electron energy-loss spectroscopy (EELS) was used to measure the electronic bandgap. The EELS measurements were performed at 80 kV with a ThermoFisher USA (formerly FEI Co) Titan Themis Z (40–300 kV) transmission electron microscopy (TEM). The TEM was equipped with a double Cs (spherical aberration) corrector, a high brightness electron gun (*x*-FEG), an electron beam monochromator, and a Gatan Quantum 966 imaging filter (GIF). Low-loss spectra were acquired in microprobe scanning TEM (STEM) mode with about 1 mrad semi convergence angle (4 nm probe). The TEM lamella is around 100 nm thick. The spectrum was captured with resolution of 5 meV and a zero-loss peak full width at half maximum (FWHM) of 50 meV utilizing a monochromator as has been optimized by Lopatin *et al* [18].

Finally, the valence band and a few core level energies were measured using a Kratos AXIS Ultra XPS. The XPS data was then used to calculate VBO of BGaN with AlN and GaN using equation (2) and equation (3). Since our samples are insulating, charge correction is applied by fixing the C 1s peak at 284.8 eV binding energy [19]. Using this, the Fermi level is assumed at 0 eV binding energy. This serves as an effective reference energy for each XPS scan—it has been reported that the Fermi level is expected to be within the window of $0 \pm 0.3\ \text{eV}$ given this reference (C 1s peak) [20]. The 0.3 eV error is not in the C 1s reference, so it does not propagate to the band alignment. However, the error in this measurement comes from the electron energy analyzer's precision which is $\pm 0.1\ \text{eV}$.

3. Results and discussion

The BGaN film is epitaxially grown on the AlN template and is (002)-oriented. Figure 2(a) shows the XRD 2θ - ω scan of the BGaN/AlN sample with an angular distance of 0.81° between the BGaN and the AlN (002) peaks. This gives us an approximate B composition of 9.7%. The assumed lattice parameters are in the inset of figure 2(a), which are in agreement with literature accepted values [21, 22]. Both bandgap and band offset are dependent on B composition. The bandgap of our sample is first examined using several techniques. Figure 2(b) shows the Tauc plot and the photodetector responsivity curve. Both results in figure 2(b) give nearly the same optical bandgap of the BGaN material. The Tauc plot gives a bandgap of 3.58 eV and the photodetector peak is at 3.51 eV.

The responsivity peak has multiple adjacent near band edge peaks which could be the result of either the presence of another phase or more likely point defects and impurities [10]. To investigate the phase purity of the sample, cross-sectional STEM images are taken (figure 3(a)). Like earlier reports, the image shows a wurtzite material rich in stacking faults which enable the presence of zincblende inclusions in the film [23–25]. The sample is then measured using EELS to investigate its bandgap and aid in the interpretation of the band alignment.

It was found that the EELS signal is quite noisy for the BGaN film due to the material's quality. As a result, the measurement data is smoothed using a linear Savitzky–Golay method with 10 points of window [26, 27]. The number of points is chosen such that the resolution of the spectra is not reduced beyond the FWHM of the ZLP (50 meV), which is taken as the measurement error. The EELS signal is extracted from an area of $\sim 500 \times 100\ \text{N m}^2$ from either side of the BGaN–AlN interface.

To extract the bandgaps, the first derivative of the smoothed curves is then fitted with a Gaussian peak. The position of the peak is considered the bandgap [26]. Due to the higher noise in the BGaN spectrum and to avoid the influence of the near band edge peaks, the measured data is smoothed with a window of 100 points before taking the derivative (not shown). The EELS bandgaps for the AlN and BGaN layers are 5.96 eV and

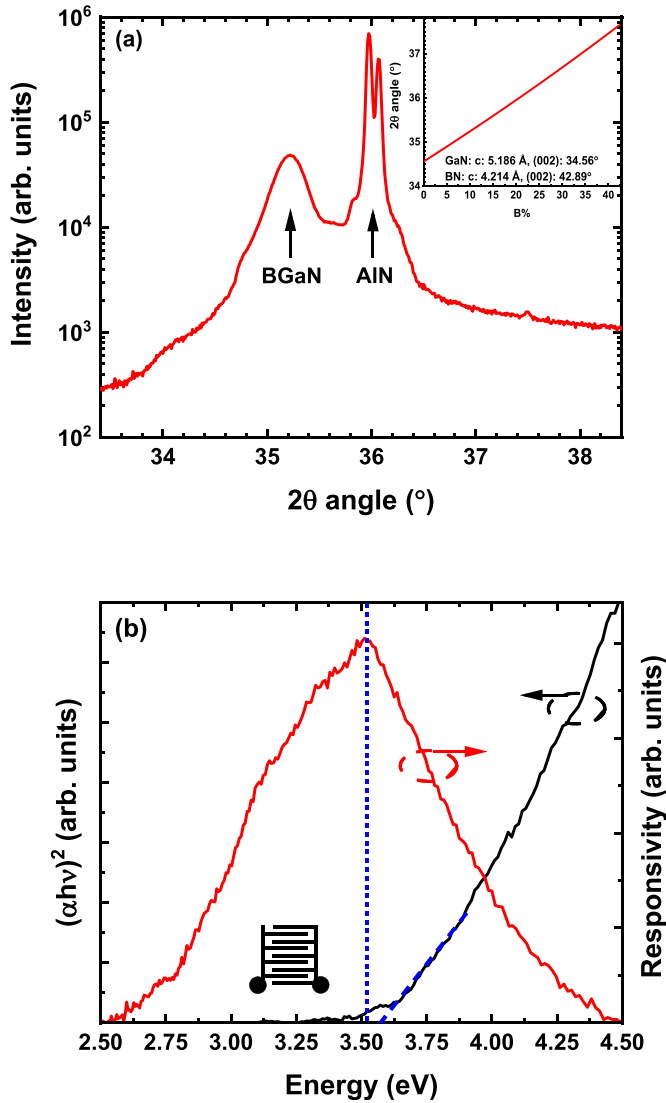


Figure 2. (a) 2θ - ω XRD scan showing the (002) peaks for AlN and BGaN. The AlN double-peak feature is due to x-rays containing both $K_{\alpha 1}$ and $K_{\alpha 2}$ emissions. The inset in (a) shows the calculated 2θ at different compositions based on linear interpolation of the indicated lattice constants. (b) Tauc plot and responsivity spectrum of the BGaN film showing similar bandgap values. The inset in (b) is a schematic of the interdigitated MSM photodetector (not to scale). The thickness is 120 nm in both (a) and (b).

3.55 eV, respectively (figures 3(b) and (c)). Since the major features of the spectra are not changed by the smoothing, the error is assumed to be 50 meV (equal to the FWHM of the ZLP).

Finally, the band alignment of the grown BGaN film is investigated by XPS. To align BGaN with AlN, the Kraut method is initially used. This method gives the clearest picture regarding the band alignment, so its result is later used to validate the alignment with GaN. To perform the measurements for this method, three samples are grown: ‘bulk’ AlN, ‘bulk’ BGaN, and BGaN/AlN interface (figure 4(a)). A fourth sample of AlN/BGaN interface is also grown for cross-validation. Figure 4(c) shows the measured XPS spectra and

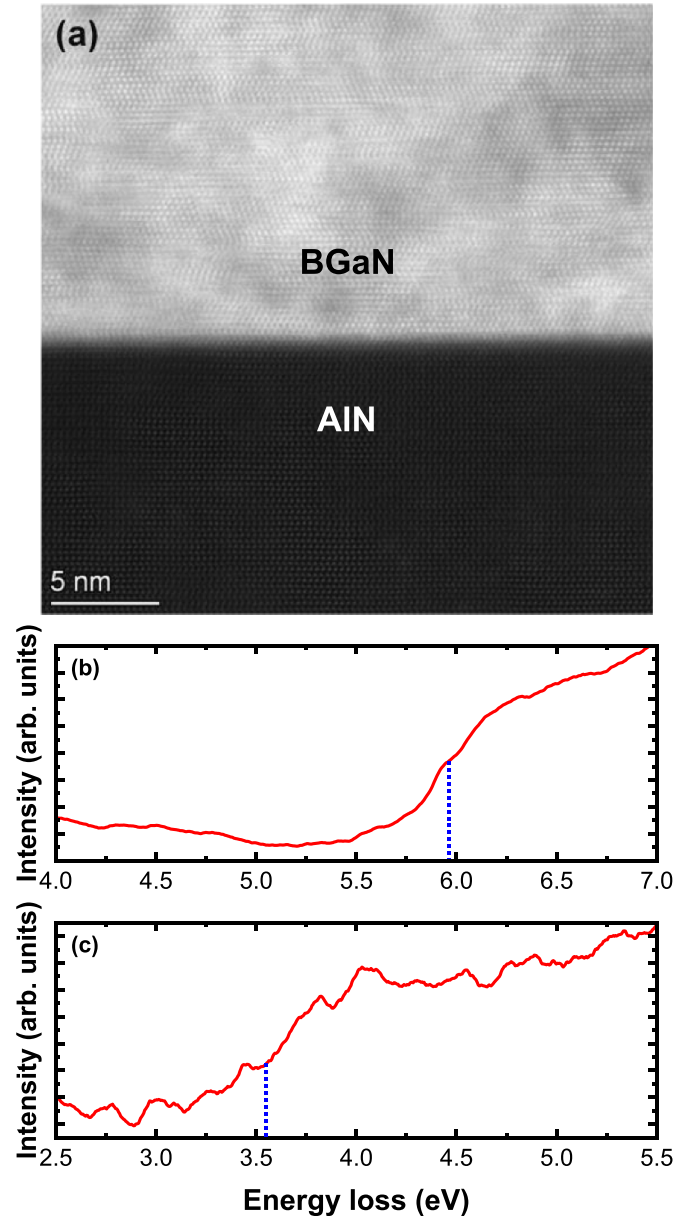


Figure 3. (a) High resolution dark field STEM image near the BGaN/AlN interface. (b) and (c) The smoothed EELS spectra of AlN and BGaN, respectively, with the bandgaps highlighted by the dotted lines. The window of points for the smoothing process is 10 (equal to 50 meV).

the difference in energy levels for each sample. These values can be directly put into equation (2) to get a VBO of -1.1 eV. The error here is taken as the precision of the XPS instrument which is ± 0.1 eV. The cross-validation sample’s VBO result is -1.2 eV, which is within the error of the measurement. The cross-validation sample has lower material quality, so -1.1 eV is taken as the VBO.

The alignment of BGaN and AlN is relatively straightforward when the growth conditions of each sample are optimized. However, the alignment of BGaN with GaN, as in the case of our sample in figure 4(b), is not easily achieved using the Kraut method. This is due to the core levels in the interface

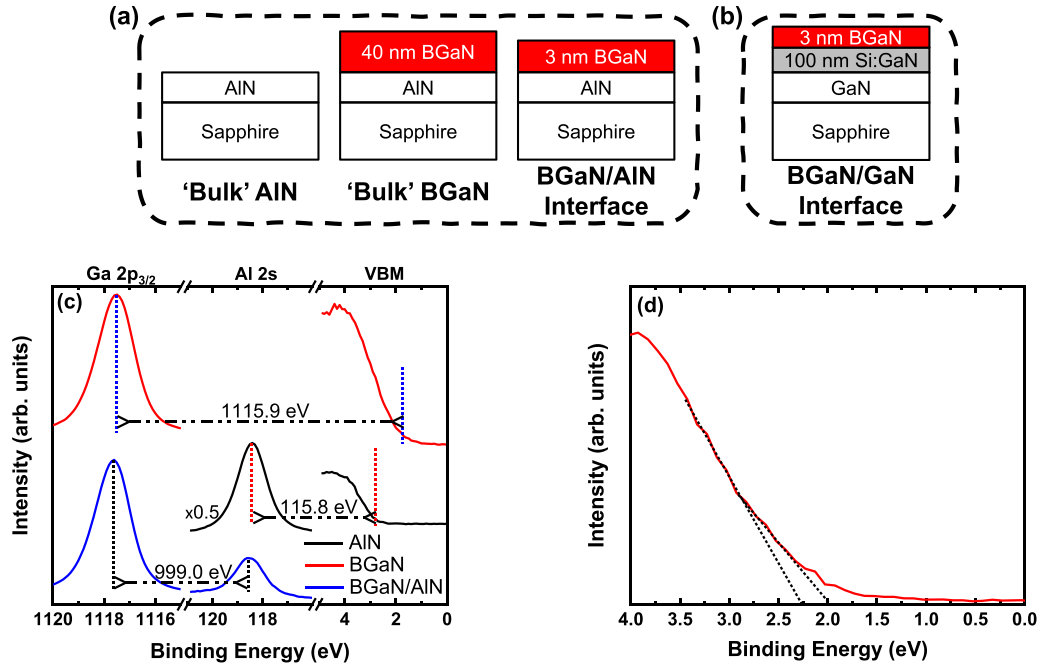


Figure 4. (a) Schematic of the samples needed for the alignment of BGaN/AlN using the method in equation (2). The AlN layers are part of 1.5 μm thick templates. (b) Schematic of the BGaN/GaN sample. The GaN regrowth layer is lightly Si doped ($\sim 10^{17}/\text{cm}^3$), and the GaN underlayer is a 2.5 μm thick template. (c) The measured XPS spectra of the samples in (a). (d) The measured spectrum of the sample in (b) in the low binding energy range. The dashed lines in (d) correspond to the valence band edges of the GaN and BGaN layers within the sample.

sample belonging to the same atoms (Ga and N). The only core level that can distinguish BGaN from GaN is that of the B atom. The Si doping within the GaN layer is below the detection limit of the XPS instrument, so it is difficult to align the interface according to equation (2) (figures 1(b) and (c)).

A similar issue led Mickevicius *et al* to oversimplify the Kraut method and use an equation that may seem identical to equation (3) at first glance [9]. However, what they missed is that the measured VBM are referenced to different Fermi levels since they only measured 'bulk' samples (figure 1(b)). Therefore, in this study, we perform the measurement only on interface samples such that the energies are referenced properly.

This method makes the alignment of GaN with BGaN on its surface analogous to the alignment of a Si with native SiO₂ on its surface [7, 8]. This approach is relatively easy to apply to a heterojunction between materials with different bandgaps and valence band positions even in the absence of two distinct core levels of each material. However, this method aligns the heterojunction at the interface instead of the bulk materials (equation (3)). This means that band bending due to interface states and polarization is not taken into account by this method as in the case of alignment using the Kraut method. Furthermore, this method is not so straightforward when the bandgaps and the VBM of the two materials are close. This is, unfortunately, the case for BGaN and GaN. Therefore, to resolve the BGaN/GaN VBO, we utilize a novel statistical technique to process the low binding energy XPS data in

figure 4(d). This technique could be described as follows: (1) a 0.2 eV-wide section of the valence edge is fitted with a line. (2) The x -intercept of the line is taken as a data point. (3) The fitted section is shifted by 0.1 eV and another x -intercept is taken. This is repeated until the full length of the valence band is processed. Once all the data points are taken, they are plotted in a histogram as in figure 5(a). In the histogram we can clearly find two peaks that correspond to two linear fits of the valence band edge. Those lines are plotted in figure 4(d) and show the most likely VBM positions. A difference of -0.3 eV in their x -intercept values corresponds to the VBO of the BGaN/GaN interface (equation (3)). See supplementary material for an analysis of the robustness of this statistical method.

Finally, a flat band model for the alignment result of B_{0.097}Ga_{0.903}N with AlN and GaN is made in figure 5(b) to summarize the band structure results. The results show a type-I alignment for the BGaN/AlN heterojunction and a type-II alignment for the BGaN/GaN junction. These results are qualitatively in agreement with the density-functional theory (DFT) results by Ota *et al*, but are different from the DFT results by Al Sulami *et al* [28, 29]. Table 1 summarizes the comparison between our experimental results and the previous two DFT results. Additionally, this flat band representation allows us to infer the alignment of the more studied material pair GaN/AlN. As table 1 and figure 5(b) show, the inferred VBO and CBO have values of 0.8 eV and 1.8 eV, which almost perfectly matches the commonly cited 30:70 VBO:CBO ratio for the AlGaN material system [30, 31].

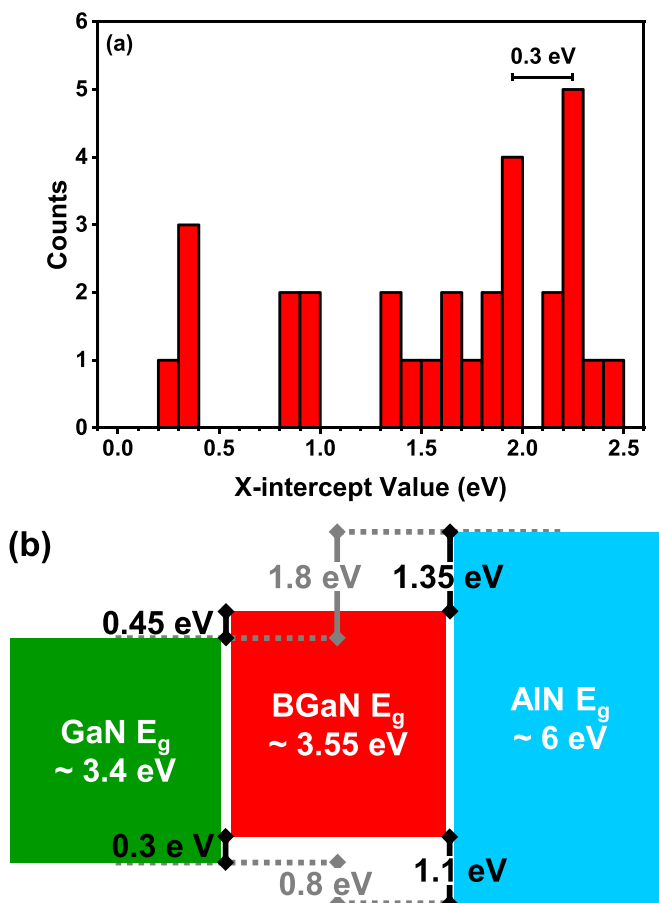


Figure 5. (a) Histogram representing the results of our statistical method for finding the VBM of BGaN and GaN layers from the low binding energy region of the XPS spectrum. (b) Summary of the alignments of $B_{0.097}Ga_{0.903}N$ with AlN and GaN. The literature accepted values of the gaps of GaN and AlN are used to find the CBO values with BGaN.

Table 1. Summary of absolute values of VBOs both as experimentally measured here and theoretically calculated using DFT [28, 29]. The GaN/AlN offset is inferred by the two measurements with BGaN. The theoretical calculation results are for BGaN with composition of 12.5%, which is slightly different from the composition here.

References	BGaN/AlN	BGaN/GaN	GaN/AlN
This work	1.1 eV	0.3 eV	0.8 eV ^a
Al Sulami et al [29]	2.735 eV	1.81 eV	0.925 eV
Ota et al [28]	0.77 eV	0.12 eV	0.65 eV

^a Inferred offset.

4. Conclusion

We have studied the band structure of BGaN in detail using several characterization methods. A B composition of 9.7% was estimated using the peak position of the XRD scan. The bandgap is studied using UV–Vis transmittance, MSM photodetector responsivity and EELS spectra. The bandgap values using all the methods agree with the EELS value of 3.55 ± 0.05 eV. Using STEM, the material is found to be

wurtzite with stacking faults in the vertical (002) direction, which enable the presence of the zincblende phase within the crystal. Finally, the band alignments of BGaN with AlN and GaN are studied in detail. The BGaN/AlN alignment is straightforward using the traditional alignment technique by XPS. However, due to similarities in the core levels of BGaN and GaN and their close valence edges, a novel statistical technique is used for this alignment. This technique is found to give a similar precision to that of the XPS electron energy analyzer. We believe this method could give even better precision with higher resolution measurements. Additionally, this method should be applicable to other III-nitride alloys and other material systems.

Data availability statement

All data that support the findings of this study are included within the article (and any supplementary files).

Acknowledgments

The authors acknowledge the support of the KAUST Baseline Fund under Grant No. BAS/1/1664-01-01, Competitive Research under Grant Nos. URF/1/3437-01-01 and URF/1/3771-01-01, and the GCC Research Council under Grant No. REP/1/3189-01-01.

ORCID iDs

F AlQatari <https://orcid.org/0000-0001-7620-4569>

X Tang <https://orcid.org/0000-0002-0138-7206>

X Li <https://orcid.org/0000-0002-4434-365X>

References

- [1] Trasatti S and Parsons R 1986 Interphases in systems of conducting phases (Recommendations 1985) *Pure Appl. Chem.* **58** 437
- [2] Xu X, Liu X, Guo Y, Wang J, Song H, Yang S, Wei H, Zhu Q and Wang Z 2010 Influence of band bending and polarization on the valence band offset measured by x-ray photoelectron spectroscopy *J. Appl. Phys.* **107** 104510
- [3] Morar J F, Batson P E and Tersoff J 1993 Heterojunction band lineups in Si-Ge alloys using spatially resolved electron-energy-loss spectroscopy *Phys. Rev. B* **47** 4107
- [4] Sun H, Park Y J, Li K-H, Torres Castaneda C, Alowayed A, Detchprohm T, Dupuis R D and Li X 2017 Band alignment of $B_{0.14}Al_{0.86}N/Al_{0.7}Ga_{0.3}N$ heterojunction *Appl. Phys. Lett.* **111** 122106
- [5] Wang J et al 2014 Evidence of Type-II band alignment in III-nitride semiconductors: experimental and theoretical investigation for $In_{0.17}Al_{0.83}N/GaN$ heterostructures *Sci. Rep.* **4** 6521
- [6] Kraut E, Grant R, Waldrop J and Kowalczyk S 1980 Precise determination of the valence-band edge in x-ray photoemission spectra: application to measurement of semiconductor interface potentials *Phys. Rev. Lett.* **44** 1620
- [7] Grunthaner F and Grunthaner P 1986 Chemical and electronic structure of the SiO_2/Si interface *Mater. Sci. Rep.* **1** 65
- [8] Alay J L and Hirose M 1997 The valence band alignment at ultrathin SiO_2/Si interfaces *J. Appl. Phys.* **81** 1606

- [9] Mickevičius J, Andrulevicius M, Ligor O, Kadys A, Tomašiūnas R, Tamulaitis G and Pavelescu E 2019 Type-II band alignment of low-boron-content BGaN/GaN heterostructures *J. Phys. D: Appl. Phys.* **52** 325105
- [10] AlQatari F, Liao C-H and Li X 2022 Demonstration of MOCVD-grown BGaN with over 10% boron composition *AIP Adv.* **12** 085318
- [11] Flack T J, Pushpakaran B N and Bayne S B 2016 GaN technology for power electronic applications: a review *J. Electron. Mater.* **45** 2673
- [12] Hu J, Zhang Y, Sun M, Piedra D, Chowdhury N and Palacios T 2018 Materials and processing issues in vertical GaN power electronics *Mater. Sci. Semicond. Proc.* **78** 75
- [13] Yu H-C, Zheng Z-W, Mei Y, Xu R-B, Liu J-P, Yang H, Zhang B-P, Lu T-C and Kuo H-C 2018 Progress and prospects of GaN-based VCSEL from near UV to green emission *Prog. Quantum Electron.* **57** 1
- [14] Zhang H et al 2022 Monolithic GaN optoelectronic system on a Si substrate *Appl. Phys. Lett.* **121** 181103
- [15] Denton A R and Ashcroft N W 1991 Vegard's law *Phys. Rev. A* **43** 3161
- [16] Ajay A et al 2016 Ge doping of GaN beyond the Mott transition *J. Phys. D: Appl. Phys.* **49** 445301
- [17] Xie F, Lu H, Xiu X, Chen D, Han P, Zhang R and Zheng Y 2011 Low dark current and internal gain mechanism of GaN MSM photodetectors fabricated on bulk GaN substrate *Solid-State Electron.* **57** 39
- [18] Lopatin S, Cheng B, Liu W-T, Tsai M-L, He J-H and Chuvilin A 2018 Optimization of monochromated TEM for ultimate resolution imaging and ultrahigh resolution electron energy loss spectroscopy *Ultramicroscopy* **184** 109
- [19] Swift P 1982 Adventitious carbon—the panacea for energy referencing? *Surf. Interface Anal.* **4** 47
- [20] Barr T L and Seal S 1995 Nature of the use of adventitious carbon as a binding energy standard *J. Vac. Sci. Technol. A* **13** 1239
- [21] Bundy F P and Wentorf Jr R H 2004 Direct Transformation of Hexagonal Boron Nitride to Denser Forms *J. Chem. Phys.* **38** 1144
- [22] Liu K, Sun H, AlQatari F, Guo W, Liu X, Li J, Torres Castanedo C G and Li X 2017 Wurtzite BAlN and BGaN alloys for heterointerface polarization engineering *Appl. Phys. Lett.* **111** 222106
- [23] Gautier S et al 2011 Deep structural analysis of novel BGaN material layers grown by MOVPE *J. Cryst. Growth* **315** 288
- [24] Gunning B P, Moseley M W, Koleske D D, Allerman A A and Lee S R 2017 Phase degradation in $B_xGa_{1-x}N$ films grown at low temperature by metalorganic vapor phase epitaxy *J. Cryst. Growth* **464** 190
- [25] Nakano T et al 2021 Effective neutron detection using vertical-type BGaN diodes *J. Appl. Phys.* **130** 124501
- [26] Brescia R, Toso S, Ramasse Q, Manna L, Shamsi J, Downing C, Calzolari A and Bertoni G 2020 Bandgap determination from individual orthorhombic thin cesium lead bromide nanosheets by electron energy-loss spectroscopy *Nanoscale Horiz.* **5** 1610
- [27] Press W H and Teukolsky S A 1990 Savitzky-Golay smoothing filters *Comput. Phys.* **4** 669
- [28] Ota Y, Imura M, Banal R G and Koide Y 2022 Natural band alignment of BAlN and BGaN alloys *J. Phys. D: Appl. Phys.* **55** 455102
- [29] Al Sulami A, AlQatari F and Li X 2020 Band alignments of emerging wurtzite BAlN and BGaN semiconductors (arXiv:2005.08407)
- [30] Cingolani R, Colí G, Rinaldi R, Calcagnile L, Tang H, Botchkarev A, Kim W, Salvador A and Morkoç H 1998 One- and two-photon absorption spectroscopy of GaN/AlGaIn quantum wells *Physica E* **2** 539
- [31] Sang L et al 2014 Band offsets of non-polar A-plane GaN/AlN and AlN/GaN heterostructures measured by x-ray photoemission spectroscopy *Nanoscale Res. Lett.* **9** 470